A TECHNICAL DETAILS OF SPECTRAL LEARNING WITH WILD DATA

Theorem A.1. *(Recap of Theorem 3.1) Let $f_x = \sqrt{w_x} f(x)$ for some function f. Recall η_u, η_l are coefficients defined in Eq. 1. Then, the loss function $\mathcal{L}_{\mathrm{mf}}(F, A)$ is equivalent to the following loss function for f, which we term* ***Spectral Learning with Wild Data (SLW)****:*

$$\mathcal{L}_{SLW}(f) \triangleq -2\eta_u \mathcal{L}_1(f) - 2\eta_l \mathcal{L}_2(f) + \eta_u^2 \mathcal{L}_3(f) + 2\eta_u \eta_l \mathcal{L}_4(f) + \eta_l^2 \mathcal{L}_5(f), \tag{14}$$

where

$$\begin{aligned}
\mathcal{L}_1(f) &= \sum_{i \in \mathcal{Y}_l} \mathop{\mathbb{E}}_{\substack{\bar{x}_l \sim \mathbb{P}_{l_i}, \bar{x}'_l \sim \mathbb{P}_{l_i}, \\ x \sim \mathcal{T}(\cdot|\bar{x}_l), x^+ \sim \mathcal{T}(\cdot|\bar{x}'_l)}} \left[f(x)^\top f\left(x^+\right) \right], \\
\mathcal{L}_2(f) &= \mathop{\mathbb{E}}_{\substack{\bar{x}_u \sim \mathbb{P}, \\ x \sim \mathcal{T}(\cdot|\bar{x}_u), x^+ \sim \mathcal{T}(\cdot|\bar{x}_u)}} \left[f(x)^\top f\left(x^+\right) \right], \\
\mathcal{L}_3(f) &= \sum_{i,j \in \mathcal{Y}_l} \mathop{\mathbb{E}}_{\substack{\bar{x}_l \sim \mathbb{P}_{l_i}, \bar{x}'_l \sim \mathbb{P}_{l_j}, \\ x \sim \mathcal{T}(\cdot|\bar{x}_l), x^- \sim \mathcal{T}(\cdot|\bar{x}'_l)}} \left[\left(f(x)^\top f\left(x^-\right) \right)^2 \right], \\
\mathcal{L}_4(f) &= \sum_{i \in \mathcal{Y}_l} \mathop{\mathbb{E}}_{\substack{\bar{x}_l \sim \mathbb{P}_{l_i}, \bar{x}_u \sim \mathbb{P}, \\ x \sim \mathcal{T}(\cdot|\bar{x}_l), x^- \sim \mathcal{T}(\cdot|\bar{x}_u)}} \left[\left(f(x)^\top f\left(x^-\right) \right)^2 \right], \\
\mathcal{L}_5(f) &= \mathop{\mathbb{E}}_{\substack{\bar{x}_u \sim \mathbb{P}, \bar{x}'_u \sim \mathbb{P}, \\ x \sim \mathcal{T}(\cdot|\bar{x}_u), x^- \sim \mathcal{T}(\cdot|\bar{x}'_u)}} \left[\left(f(x)^\top f\left(x^-\right) \right)^2 \right].
\end{aligned}$$

Proof. We can expand $\mathcal{L}_{\mathrm{mf}}(F, A)$ and obtain

$$\begin{aligned}
\mathcal{L}_{\mathrm{mf}}(F, A) &= \sum_{x, x' \in \mathcal{X}} \left(\frac{w_{xx'}}{\sqrt{w_x w_{x'}}} - f_x^\top f_{x'} \right)^2 \\
&= \text{const} + \sum_{x, x' \in \mathcal{X}} \left(-2 w_{xx'} f(x)^\top f\left(x'\right) + w_x w_{x'} \left(f(x)^\top f\left(x'\right) \right)^2 \right),
\end{aligned}$$

where $f_x = \sqrt{w_x} f(x)$ is a re-scaled version of $f(x)$. At a high level, we follow the proof in HaoChen et al. (2021), while the specific form of loss varies with the different definitions of positive/negative pairs. The form of $\mathcal{L}_{\mathrm{SLW}}(f)$ is derived from plugging $w_{xx'}$ and w_x.

Recall that $w_{xx'}$ is defined by

$$w_{xx'} = \eta_u \sum_{i \in \mathcal{Y}_l} \mathbb{E}_{\bar{x}_l \sim \mathbb{P}_{l_i}} \mathbb{E}_{\bar{x}'_l \sim \mathbb{P}_{l_i}} \mathcal{T}(x|\bar{x}_l) \mathcal{T}\left(x'|\bar{x}'_l\right) + \eta_l \mathbb{E}_{\bar{x}_u \sim \mathbb{P}} \mathcal{T}(x|\bar{x}_u) \mathcal{T}\left(x'|\bar{x}_u\right),$$

and w_x is given by

$$\begin{aligned}
w_x &= \sum_{x'} w_{xx'} \\
&= \eta_u \sum_{i \in \mathcal{Y}_l} \mathbb{E}_{\bar{x}_l \sim \mathbb{P}_{l_i}} \mathbb{E}_{\bar{x}'_l \sim \mathbb{P}_{l_i}} \mathcal{T}(x|\bar{x}_l) \sum_{x'} \mathcal{T}\left(x'|\bar{x}'_l\right) + \eta_l \mathbb{E}_{\bar{x}_u \sim \mathbb{P}} \mathcal{T}(x|\bar{x}_u) \sum_{x'} \mathcal{T}\left(x'|\bar{x}_u\right) \\
&= \eta_u \sum_{i \in \mathcal{Y}_l} \mathbb{E}_{\bar{x}_l \sim \mathbb{P}_{l_i}} \mathcal{T}(x|\bar{x}_l) + \eta_l \mathbb{E}_{\bar{x}_u \sim \mathbb{P}} \mathcal{T}(x|\bar{x}_u).
\end{aligned}$$

Plugging in $w_{xx'}$ we have,

$$
\begin{aligned}
&- 2 \sum_{x,x' \in \mathcal{X}} w_{xx'} f(x)^\top f\left(x'\right) \\
=& - 2 \sum_{x,x^+ \in \mathcal{X}} w_{xx^+} f(x)^\top f\left(x^+\right) \\
=& - 2\eta_u \sum_{i \in \mathcal{Y}_l} \mathbb{E}_{\bar{x}_l \sim \mathbb{P}_{l_i}} \mathbb{E}_{\bar{x}'_l \sim \mathbb{P}_{l_i}} \sum_{x,x' \in \mathcal{X}} \mathcal{T}(x|\bar{x}_l) \mathcal{T}\left(x'|\bar{x}'_l\right) f(x)^\top f\left(x'\right) \\
&- 2\eta_l \mathbb{E}_{\bar{x}_u \sim \mathbb{P}} \sum_{x,x'} \mathcal{T}(x|\bar{x}_u) \mathcal{T}\left(x'|\bar{x}_u\right) f(x)^\top f\left(x'\right) \\
=& - 2\eta_u \sum_{i \in \mathcal{Y}_l} \mathop{\mathbb{E}}_{\substack{\bar{x}_l \sim \mathbb{P}_{l_i}, \bar{x}'_l \sim \mathbb{P}_{l_i}, \\ x \sim \mathcal{T}(\cdot|\bar{x}_l), x^+ \sim \mathcal{T}(\cdot|\bar{x}'_l)}} \left[f(x)^\top f\left(x^+\right)\right] \\
&- 2\eta_l \mathop{\mathbb{E}}_{\substack{\bar{x}_u \sim \mathbb{P}, \\ x \sim \mathcal{T}(\cdot|\bar{x}_u), x^+ \sim \mathcal{T}(\cdot|\bar{x}_u)}} \left[f(x)^\top f\left(x^+\right)\right] \\
=& - 2\eta_u \mathcal{L}_1(f) - 2\eta_l \mathcal{L}_2(f).
\end{aligned}
$$

Plugging w_x and $w_{x'}$ we have,

$$
\begin{aligned}
&\sum_{x,x' \in \mathcal{X}} w_x w_{x'} \left(f(x)^\top f\left(x'\right)\right)^2 \\
=& \sum_{x,x^- \in \mathcal{X}} w_x w_{x^-} \left(f(x)^\top f\left(x^-\right)\right)^2 \\
=& \sum_{x,x' \in \mathcal{X}} \left(\eta_u \sum_{i \in \mathcal{Y}_l} \mathbb{E}_{\bar{x}_l \sim \mathbb{P}_{l_i}} \mathcal{T}(x|\bar{x}_l) + \eta_l \mathbb{E}_{\bar{x}_u \sim \mathbb{P}} \mathcal{T}(x|\bar{x}_u)\right) \\
&\qquad \cdot \left(\eta_u \sum_{j \in \mathcal{Y}_l} \mathbb{E}_{\bar{x}'_l \sim \mathbb{P}_{l_j}} \mathcal{T}(x^-|\bar{x}'_l) + \eta_l \mathbb{E}_{\bar{x}'_u \sim \mathbb{P}} \mathcal{T}(x^-|\bar{x}'_u)\right) \left(f(x)^\top f\left(x^-\right)\right)^2 \\
=& \eta_u^2 \sum_{x,x^- \in \mathcal{X}} \sum_{i \in \mathcal{Y}_l} \mathbb{E}_{\bar{x}_l \sim \mathbb{P}_{l_i}} \mathcal{T}(x|\bar{x}_l) \sum_{j \in \mathcal{Y}_l} \mathbb{E}_{\bar{x}'_l \sim \mathbb{P}_{l_j}} \mathcal{T}(x^-|\bar{x}'_l) \left(f(x)^\top f\left(x^-\right)\right)^2 \\
&+ 2\eta_u \eta_l \sum_{x,x^- \in \mathcal{X}} \sum_{i \in \mathcal{Y}_l} \mathbb{E}_{\bar{x}_l \sim \mathbb{P}_{l_i}} \mathcal{T}(x|\bar{x}_l) \mathbb{E}_{\bar{x}_u \sim \mathbb{P}} \mathcal{T}(x^-|\bar{x}_u) \left(f(x)^\top f\left(x^-\right)\right)^2 \\
&+ \eta_l^2 \sum_{x,x^- \in \mathcal{X}} \mathbb{E}_{\bar{x}_u \sim \mathbb{P}} \mathcal{T}(x|\bar{x}_u) \mathbb{E}_{\bar{x}'_u \sim \mathbb{P}} \mathcal{T}(x^-|\bar{x}'_u) \left(f(x)^\top f\left(x^-\right)\right)^2 \\
=& \eta_u^2 \sum_{i \in \mathcal{Y}_l} \sum_{j \in \mathcal{Y}_l} \mathop{\mathbb{E}}_{\substack{\bar{x}_l \sim \mathbb{P}_{l_i}, \bar{x}'_l \sim \mathbb{P}_{l_j}, \\ x \sim \mathcal{T}(\cdot|\bar{x}_l), x^- \sim \mathcal{T}(\cdot|\bar{x}'_l)}} \left[\left(f(x)^\top f\left(x^-\right)\right)^2\right] \\
&+ 2\eta_u \eta_l \sum_{i \in \mathcal{Y}_l} \mathop{\mathbb{E}}_{\substack{\bar{x}_l \sim \mathbb{P}_{l_i}, \bar{x}_u \sim \mathbb{P}, \\ x \sim \mathcal{T}(\cdot|\bar{x}_l), x^- \sim \mathcal{T}(\cdot|\bar{x}_u)}} \left[\left(f(x)^\top f\left(x^-\right)\right)^2\right] \\
&+ \eta_l^2 \mathop{\mathbb{E}}_{\substack{\bar{x}_u \sim \mathbb{P}, \bar{x}'_u \sim \mathbb{P}, \\ x \sim \mathcal{T}(\cdot|\bar{x}_u), x^- \sim \mathcal{T}(\cdot|\bar{x}'_u)}} \left[\left(f(x)^\top f\left(x^-\right)\right)^2\right] \\
=& \eta_u^2 \mathcal{L}_3(f) + 2\eta_u \eta_l \mathcal{L}_4(f) + \eta_l^2 \mathcal{L}_5(f).
\end{aligned}
$$

□

B IMPACT OF SEMANTIC OOD DATA

In our main analysis in Section 4, we consider semantic OOD to be from a different domain. Alternatively, instances of semantic OOD data can come from the same domain as covariate OOD data. In this section, we provide a complete picture by contrasting these two cases.

Setup. In Figure 5, we illustrate two scenarios where the semantic OOD data has either a different or the same domain label as covariate OOD data. Other setups are the same as Sec. 4.3.

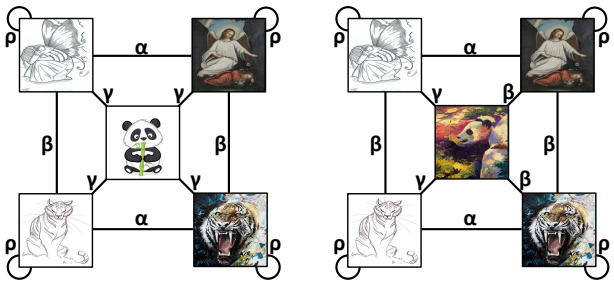

(a) $d(\text{panda}) \neq \text{painting}$ (b) $d(\text{panda}) = \text{painting}$

Figure 5: Illustration of 5 nodes graph and the augmentation probability defined by classes and domains. Figure (a) illustrates the scenario where semantic OOD data has a different domain from covariate OOD. Figure (b) depicts the case where semantic OOD and covariate OOD share the same domain.

Adjacency matrix. The adjacency matrix for scenario (a) has been derived in Eq. 11. For the alternative scenario (b) where semantic OOD shares the same domain as the covariate OOD, we can derive the analytic form of adjacency matrix A_1.

$$\eta_u A_1^{(u)} = \begin{bmatrix} \rho^2+\beta^2+\alpha^2+2\gamma^2 & 2\rho\beta+\gamma^2+2\gamma\alpha & 2\rho\alpha+3\gamma\beta & 2\alpha\beta+\gamma\beta+2\gamma\rho & \alpha\beta+2\gamma(\beta+\rho) \\ 2\rho\beta+\gamma^2+2\gamma\alpha & \rho^2+\beta^2+\alpha^2+2\gamma^2 & 2\alpha\beta+\gamma\beta+2\gamma\rho & 2\rho\alpha+3\gamma\beta & \alpha\beta+2\gamma(\beta+\rho) \\ 2\rho\alpha+3\gamma\beta & 2\alpha\beta+\gamma\beta+2\gamma\rho & \rho^2+2\beta^2+\alpha^2+\gamma^2 & 2\rho\beta+\beta^2+2\gamma\alpha & 2\rho\beta+\beta^2+\gamma^2+\gamma\alpha \\ 2\alpha\beta+\gamma\beta+2\gamma\rho & 2\alpha\rho+3\gamma\beta & 2\rho\beta+\beta^2+2\gamma\alpha & \rho^2+2\beta^2+\alpha^2+\gamma^2 & 2\rho\beta+\beta^2+\gamma^2+\gamma\alpha \\ \alpha\beta+2\gamma(\beta+\rho) & \alpha\beta+2\gamma(\beta+\rho) & 2\rho\beta+\beta^2+\gamma^2+\gamma\alpha & 2\rho\beta+\beta^2+\gamma^2+\gamma\alpha & \rho^2+2\beta^2+2\gamma^2 \end{bmatrix} \tag{15}$$

$$A_1 = \frac{1}{C_1}(\eta_l A_1^{(l)} + \eta_u A_1^{(u)}) = \frac{1}{C_1}\Big(\begin{bmatrix} \rho^2+\beta^2 & 2\rho\beta & \rho\alpha+\gamma\beta & \alpha\beta+\gamma\rho & \gamma(\beta+\rho) \\ 2\rho\beta & \rho^2+\beta^2 & \alpha\beta+\gamma\rho & \rho\alpha+\gamma\beta & \gamma(\beta+\rho) \\ \rho\alpha+\gamma\beta & \alpha\beta+\gamma\rho & \alpha^2+\gamma^2 & 2\gamma\alpha & \gamma(\gamma+\alpha) \\ \alpha\beta+\gamma\rho & \rho\alpha+\gamma\beta & 2\gamma\alpha & \alpha^2+\gamma^2 & \gamma(\gamma+\alpha) \\ \gamma(\beta+\rho) & \gamma(\beta+\rho) & \gamma(\gamma+\alpha) & \gamma(\gamma+\alpha) & 2\gamma^2 \end{bmatrix} + \eta_u A_1^{(u)} \Big), \tag{16}$$

where C_1 is the normalization constant to ensure the summation of weights amounts to 1. Each row or column encodes connectivity associated with a specific sample, ordered by: angel sketch, tiger sketch, angel painting, tiger painting, and panda. We refer readers to the Appendix D.2 for the detailed derivation.

Main analysis. Following the same assumption in Sec. 4.3, we are primarily interested in analyzing the difference of the representation space derived from A and A_1 and put analysis on the top-3 eigenvectors $\widehat{V}_1 \in \mathbb{R}^{5\times 3}$.

Theorem B.1. *Denote $\alpha' = \frac{\alpha}{\rho}$ and $\beta' = \frac{\beta}{\rho}$ and assume $\eta_u = 5, \eta_l = 1$, we have:*

$$\widehat{V}_1 = \begin{bmatrix} \sqrt{2} & \sqrt{2} & 1 & 1 & 1 \\ a(\widehat{\lambda}_2) & a(\widehat{\lambda}_2) & b(\widehat{\lambda}_2) & b(\widehat{\lambda}_2) & 1 \\ c(\widehat{\lambda}_3) & -c(\widehat{\lambda}_3) & -1 & 1 & 0 \end{bmatrix}^\top \cdot R, \quad \mathcal{E}(f_1) = 0, \text{ if } \alpha > 0, \beta > 0. \tag{17}$$

where $a(\lambda) = \frac{\sqrt{2}(1-6\beta'-\lambda)}{8\beta'}, b(\lambda) = \frac{4\beta'-1+\lambda}{4\beta'}, c(\lambda) = \frac{\sqrt{2}(1-3\alpha'-6\beta'-\lambda)}{3\alpha'}$. R is a diagonal matrix that normalizes the eigenvectors to unit norm and $\widehat{\lambda}_2, \widehat{\lambda}_3$ are the 2nd and 3rd highest eigenvalues.

Interpretation. When semantic OOD shares the same domain as covariate OOD, the OOD generalization error $\mathcal{E}(f_1)$ can be reduced to 0 as long as α and β are positive. This generalization ability shows that semantic OOD and covariate OOD sharing the same domain could benefit OOD generalization. We empirically verify our theory in Section E.4.

Theorem B.2. *Denote $\alpha' = \frac{\alpha}{\rho}$ and $\beta' = \frac{\beta}{\rho}$ and assume $\eta_u = 5, \eta_l = 1$, we have:*

$$\mathcal{S}(f) - \mathcal{S}(f_1) \begin{cases} > 0 & \text{, if } \alpha', \beta' \in \textit{black area in Figure 6 (b)}; \\ < 0 & \text{, if } \alpha', \beta' \in \textit{white area in Figure 6 (b)}. \end{cases} \tag{18}$$

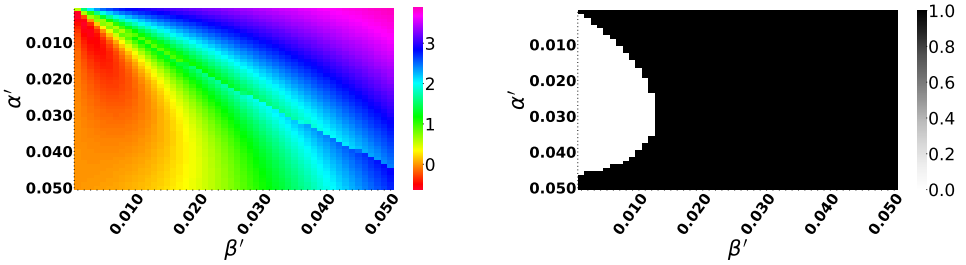

(a) Heatmap of $\mathcal{S}(f) - \mathcal{S}(f_1)$ (b) Heatmap of $\mathbb{1}(\mathcal{S}(f) - \mathcal{S}(f_1))$

Figure 6: Visualization of the separability difference between two cases defined in Figure 5 (a) and Figure 5 (b). Figure 6 (a) utilizes a heatmap to depict the distribution, while Figure 6 (a) uses the indicator function.

Interpretation. If $\alpha', \beta' \in$ black area in Figure 6 (b) and semantic OOD comes from a different domain, this would increase the separability between ID and semantic OOD, which benefits OOD detection. If $\alpha', \beta' \in$ white area in Figure 6 (b) and semantic OOD comes from a different domain, this would impair OOD detection.

C Impacts of ID Labels on OOD Generalization and Detection

Compared to spectral contrastive loss proposed by HaoChen et al. (2021), we utilize ID labels in the pre-training. In this section, we analyze the impacts of ID labels on the OOD generalization and detection performance.

Following the same assumption in Sec. 4.3, we are primarily interested in analyzing the difference of the representation space derived from A and $A^{(u)}$ and put analysis on the top-3 eigenvectors $\widehat{V}^{(u)} \in \mathbb{R}^{5\times 3}$. Detailed derivation can be found in the Appendix D.3.

Theorem C.1. *Assume $\eta_u = 5, \eta_l = 1$, we have:*

$$\widehat{V}^{(u)} = \begin{cases} \frac{1}{2}\begin{bmatrix} 1 & 1 & 1 & 1 & 0 \\ 0 & 0 & 0 & 0 & 2 \\ -1 & 1 & -1 & 1 & 0 \end{bmatrix}^\top & , \text{if } \alpha > \beta; \\ \frac{1}{2}\begin{bmatrix} 1 & 1 & 1 & 1 & 0 \\ 0 & 0 & 0 & 0 & 2 \\ -1 & -1 & 1 & 1 & 0 \end{bmatrix}^\top & , \text{if } \alpha < \beta. \end{cases}, \mathcal{E}(f^{(u)}) = \begin{cases} 0 & , \text{if } \alpha > \beta; \\ 2 & , \text{if } \alpha < \beta. \end{cases} \tag{19}$$

Interpretation. By comparing the eigenvectors $\widehat{V}$ in the supervised case (Theorem 4.1) and the eigenvectors $\widehat{V}^{(u)}$ in the self-supervised case, we find that adding ID label information transforms the performance condition from $\alpha = \beta$ to $\frac{9}{8}\alpha = \beta$. In particular, the discussion can be divided into two cases: (1) $\alpha > \beta$. (2) $\alpha < \beta$. In the first case when the connection between the class is stronger than the domain, the model could learn a perfect ID classifier based on features in the first two rows in $\widehat{V}^{(u)}$ and effectively generalize to the covariate-shifted domain (the third and fourth row in $\widehat{V}^{(u)}$), achieving perfect OOD generalization with $\mathcal{E}(f^{(u)}) = 0$. In the second case when the connection between the domain is stronger than the connection between the class, the embeddings of covariate-shifted OOD data are identical, resulting in high OOD generalization error.

Theorem C.2. *Assume $\eta_u = 5, \eta_l = 1$, we have:*

$$\mathcal{S}(f) - \mathcal{S}(f^{(u)}) > 0, \text{if } \alpha > 0, \beta > 0 \tag{20}$$

Interpretation. After incorporating ID label information, the separability between ID and semantic OOD in the learned embedding space increases as long as α and β are positive. This suggests that ID label information indeed helps OOD detection. We empirically verify our theory in Section E.4.

D TECHNICAL DETAILS OF DERIVATION

D.1 DETAILS FOR FIGURE 5 (A)

Augmentation Transformation Probability. Recall the augmentation transformation probability, which encodes the probability of augmenting an original image $\bar{x}$ to the augmented view x:

$$\mathcal{T}(x \mid \bar{x}) = \begin{cases} \rho & \text{if} \quad y(\bar{x}) = y(x), d(\bar{x}) = d(x); \\ \alpha & \text{if} \quad y(\bar{x}) = y(x), d(\bar{x}) \neq d(x); \\ \beta & \text{if} \quad y(\bar{x}) \neq y(x), d(\bar{x}) = d(x); \\ \gamma & \text{if} \quad y(\bar{x}) \neq y(x), d(\bar{x}) \neq d(x). \end{cases}$$

Thus, the augmentation matrix $\mathcal{T}$ of the toy example shown in Figure 5 (a) can be given by:

$$\mathcal{T} = \begin{bmatrix} \rho & \beta & \alpha & \gamma & \gamma \\ \beta & \rho & \gamma & \alpha & \gamma \\ \alpha & \gamma & \rho & \beta & \gamma \\ \gamma & \alpha & \beta & \rho & \gamma \\ \gamma & \gamma & \gamma & \gamma & \rho \end{bmatrix}$$

Each row or column encodes augmentation connectivity associated with a specific sample, ordered by: angel sketch, tiger sketch, angel painting, tiger painting, and panda.

Details for $A^{(u)}$ and $A^{(l)}$. Recall that the self-supervised connectivity is defined in Eq. 1. Since we have a 5-nodes graph, $A^{(u)}$ would be $\frac{1}{5}\mathcal{T}\mathcal{T}^\top$. If we assume $\eta_u = 5$, we can derive the closed-form self-supervised adjacency matrix:

$$\eta_u A^{(u)} = \begin{bmatrix} \rho^2+\beta^2+\alpha^2+2\gamma^2 & 2\rho\beta+\gamma^2+2\gamma\alpha & 2\rho\alpha+\gamma^2+2\gamma\beta & 2\alpha\beta+\gamma^2+2\gamma\rho & \gamma(\gamma+\alpha+\beta+2\rho) \\ 2\rho\beta+\gamma^2+2\gamma\alpha & \rho^2+\beta^2+\alpha^2+2\gamma^2 & 2\alpha\beta+\gamma^2+2\gamma\rho & 2\rho\alpha+\gamma^2+2\gamma\beta & \gamma(\gamma+\alpha+\beta+2\rho) \\ 2\rho\alpha+\gamma^2+2\gamma\beta & 2\alpha\beta+\gamma^2+2\gamma\rho & \rho^2+\beta^2+\alpha^2+2\gamma^2 & 2\rho\beta+\gamma^2+2\gamma\alpha & \gamma(\gamma+\alpha+\beta+2\rho) \\ 2\alpha\beta+\gamma^2+2\gamma\rho & 2\rho\alpha+\gamma^2+2\gamma\beta & 2\rho\beta+\gamma^2+2\gamma\alpha & \rho^2+\beta^2+\alpha^2+2\gamma^2 & \gamma(\gamma+\alpha+\beta+2\rho) \\ \gamma(\gamma+\alpha+\beta+2\rho) & \gamma(\gamma+\alpha+\beta+2\rho) & \gamma(\gamma+\alpha+\beta+2\rho) & \gamma(\gamma+\alpha+\beta+2\rho) & \rho^2+4\gamma^2 \end{bmatrix}$$

Then, according to the supervised connectivity defined in Eq. 2, we only compute ID-labeled data. Since we have two known classes and each class contains one sample, $A^{(l)} = \mathcal{T}_{:,1}\mathcal{T}_{:,1}^\top + \mathcal{T}_{:,2}\mathcal{T}_{:,2}^\top$. Then if we let $\eta_l = 1$, we can have the closed-form supervised adjacency matrix:

$$\eta_l A^{(l)} = \begin{bmatrix} \rho^2+\beta^2 & 2\rho\beta & \rho\alpha+\gamma\beta & \alpha\beta+\gamma\rho & \gamma(\rho+\beta) \\ 2\rho\beta & \rho^2+\beta^2 & \alpha\beta+\gamma\rho & \rho\alpha+\gamma\beta & \gamma(\rho+\beta) \\ \rho\alpha+\gamma\beta & \alpha\beta+\gamma\rho & \alpha^2+\gamma^2 & 2\gamma\alpha & \gamma(\alpha+\gamma) \\ \alpha\beta+\gamma\rho & \rho\alpha+\gamma\beta & 2\gamma\alpha & \alpha^2+\gamma^2 & \gamma(\alpha+\gamma) \\ \gamma(\rho+\beta) & \gamma(\rho+\beta) & \gamma(\alpha+\gamma) & \gamma(\alpha+\gamma) & 2\gamma^2 \end{bmatrix}$$

Details of eigenvectors $\widehat{V}$. We assume $\rho \gg \max(\alpha,\beta) \geq \min(\alpha,\beta) \gg \gamma \geq 0$, and denote $\alpha' = \frac{\alpha}{\rho}, \beta' = \frac{\beta}{\rho}$. A can be approximately given by:

$$A \approx \widehat{A} = \frac{1}{\widehat{C}} \begin{bmatrix} 2 & 4\beta' & 3\alpha' & 0 & 0 \\ 4\beta' & 2 & 0 & 3\alpha' & 0 \\ 3\alpha' & 0 & 1 & 2\beta' & 0 \\ 0 & 3\alpha' & 2\beta' & 1 & 0 \\ 0 & 0 & 0 & 0 & 1 \end{bmatrix},$$

where $\widehat{C}$ is the normalization term and equals to $7 + 12\beta' + 12\alpha'$. The squares of the minimal term (e.g., $\frac{\alpha\beta}{\rho^2}, \frac{\alpha^2}{\rho^2}, \frac{\beta^2}{\rho^2}, \frac{\gamma}{\rho} = \frac{\gamma}{\alpha}\cdot\frac{\alpha}{\rho}, \frac{\alpha\gamma}{\rho^2}$, etc) are approximated to 0.

$$\widehat{D} = \frac{1}{\widehat{C}}\text{diag}[2+4\beta'+3\alpha', 2+4\beta'+3\alpha', 1+2\beta'+3\alpha', 1+2\beta'+3\alpha', 1]$$

$$\widehat{D^{-\frac{1}{2}}} = \sqrt{\widehat{C}}\text{diag}[\frac{1}{\sqrt{2}}(1-\beta'-\frac{3}{4}\alpha'), \frac{1}{\sqrt{2}}(1-\beta'-\frac{3}{4}\alpha'), 1-\beta'-\frac{3}{2}\alpha', 1-\beta'-\frac{3}{2}\alpha', 1]$$

$$D^{-\frac{1}{2}}AD^{-\frac{1}{2}} \approx \widehat{D^{-\frac{1}{2}}}\widehat{A}\widehat{D^{-\frac{1}{2}}} = \begin{bmatrix} 1-2\beta'-\frac{3}{2}\alpha' & 2\beta' & \frac{3}{\sqrt{2}}\alpha' & 0 & 0 \\ 2\beta' & 1-2\beta'-\frac{3}{2}\alpha' & 0 & \frac{3}{\sqrt{2}}\alpha' & 0 \\ \frac{3}{\sqrt{2}}\alpha' & 0 & 1-2\beta'-3\alpha' & 2\beta' & 0 \\ 0 & \frac{3}{\sqrt{2}}\alpha' & 2\beta' & 1-2\beta'-3\alpha' & 0 \\ 0 & 0 & 0 & 0 & 1 \end{bmatrix}$$

Let $\lambda_{1,\dots,5}$ and $v_{1,\dots,5}$ be the eigenvalues and their corresponding eigenvectors of $D^{-\frac{1}{2}}AD^{-\frac{1}{2}}$. Then the concrete form of $\lambda_{1,\dots,5}$ and $v_{1,\dots,5}$ can be approximately given by:

$$\begin{aligned}
&\widehat{v}_1 = \tfrac{1}{\sqrt{6}}[\sqrt{2},\sqrt{2},1,1,0]^\top && \widehat{\lambda}_1 = 1\\
&\widehat{v}_2 = [0,0,0,0,1]^\top && \widehat{\lambda}_2 = 1\\
&\widehat{v}_3 = \tfrac{1}{\sqrt{6}}[-\sqrt{2},\sqrt{2},-1,1,0]^\top && \widehat{\lambda}_3 = 1-4\beta'\\
&\widehat{v}_4 = \tfrac{1}{\sqrt{6}}[-1,-1,\sqrt{2},\sqrt{2},0]^\top && \widehat{\lambda}_4 = 1-\tfrac{9}{2}\alpha'\\
&\widehat{v}_5 = \tfrac{1}{\sqrt{6}}[1,-1,-\sqrt{2},\sqrt{2},0]^\top && \widehat{\lambda}_5 = 1-4\beta'-\tfrac{9}{2}\alpha'
\end{aligned}$$

Since $\alpha', \beta' > 0$, we can always have $\widehat{\lambda}_1 = \widehat{\lambda}_2 > \widehat{\lambda}_3 > \widehat{\lambda}_5$ and $\widehat{\lambda}_1 = \widehat{\lambda}_2 > \widehat{\lambda}_4 > \widehat{\lambda}_5$. Then, we let $k = 3$ and $\widehat{V} \in \mathbb{R}^{5\times 3}$ is given by:

$$\widehat{V} = \begin{cases} \begin{bmatrix} \frac{1}{\sqrt{3}} & \frac{1}{\sqrt{3}} & \frac{1}{\sqrt{6}} & \frac{1}{\sqrt{6}} & 0 \\ 0 & 0 & 0 & 0 & 1 \\ -\frac{1}{\sqrt{3}} & \frac{1}{\sqrt{3}} & -\frac{1}{\sqrt{6}} & \frac{1}{\sqrt{6}} & 0 \end{bmatrix}^\top & \text{, if } \frac{9}{8}\alpha' > \beta'; \\ \begin{bmatrix} \frac{1}{\sqrt{3}} & \frac{1}{\sqrt{3}} & \frac{1}{\sqrt{6}} & \frac{1}{\sqrt{6}} & 0 \\ 0 & 0 & 0 & 0 & 1 \\ -\frac{1}{\sqrt{6}} & -\frac{1}{\sqrt{6}} & \frac{1}{\sqrt{3}} & \frac{1}{\sqrt{3}} & 0 \end{bmatrix}^\top & \text{, if } \frac{9}{8}\alpha' < \beta'. \end{cases}$$

Details of linear probing and separability evaluation. Recall that the closed-form embedding $Z = [D]^{-\frac{1}{2}}V_k\sqrt{\Sigma_k}$. Based on the derivation above, closed-form features for ID sample $Z_{\text{in}} \in \mathbb{R}^{2\times 3}$ can be approximately given by:

$$\widehat{Z}_{\text{in}} = \begin{cases} \frac{(1-\beta'-0.75\alpha')\sqrt{\widehat{C}}}{\sqrt{6}} \begin{bmatrix} 1 & 0 & -\sqrt{1-4\beta'} \\ 1 & 0 & \sqrt{1-4\beta'} \end{bmatrix} & \text{, if } \frac{9}{8}\alpha' > \beta'. \\ \frac{(1-\beta'-0.75\alpha')\sqrt{\widehat{C}}}{2\sqrt{3}} \begin{bmatrix} \sqrt{2} & 0 & -\sqrt{1-\frac{9}{2}\alpha'} \\ \sqrt{2} & 0 & -\sqrt{1-\frac{9}{2}\alpha'} \end{bmatrix} & \text{, if } \frac{9}{8}\alpha' < \beta'. \end{cases}$$

Based on the least error method, we can derive the weights of the linear classifier $M \in \mathbb{R}^{3\times 2}$,

$$\widehat{M} = (\widehat{Z}_{\text{in}}^\top \widehat{Z}_{\text{in}})^\dagger \widehat{Z}_{\text{in}}^T y_{\text{in}}$$

where $(\cdot)^\dagger$ is the Moore-Penrose inverse and y_{in} is the one-hot encoded ground truth class labels. So when $\frac{9}{8}\alpha > \beta$, the predicted probability $\widehat{y}_{\text{covariate}}$ can be given by:

$$\widehat{y}_{\text{out}}^{\text{covariate}} = \hat{Z}_{\text{out}}^{\text{covariate}} \cdot \hat{M} = \frac{(1-\beta'-\frac{3}{2}\alpha')}{1-\beta'-\frac{3}{4}\alpha'} \cdot \mathcal{I}$$

where $\mathcal{I} \in \mathbb{R}^{2\times 2}$ is an identity matrix. We notice that when $\frac{9}{8}\alpha < \beta$, the closed-form features for ID samples are identical, indicating the impossibility of learning a clear boundary to classify classes angel and tiger. Eventually, we can derive the linear probing error:

$$\mathcal{E}(f) = \begin{cases} 0 & \text{, if } \frac{9}{8}\alpha > \beta; \\ 2 & \text{, if } \frac{9}{8}\alpha < \beta. \end{cases}$$

The separability between ID data and semantic OOD data can be computed based on the closed-form embeddings $\widehat{Z}_{\text{in}}$ and $\widehat{Z}_{\text{out}}^{\text{semantic}}$:

$$\widehat{Z}_{\text{out}}^{\text{semantic}} = \sqrt{\widehat{C}} \cdot [0,1,0]$$

$$\mathcal{S}(f) = \begin{cases} (7+12\beta'+12\alpha')(\frac{1-2\beta'}{3}(1-\beta'-\frac{3}{4}\alpha')^2+1) & \text{, if } \frac{9}{8}\alpha > \beta; \\ (7+12\beta'+12\alpha')(\frac{2-3\alpha'}{8}(1-\beta'-\frac{3}{4}\alpha')^2+1) & \text{, if } \frac{9}{8}\alpha < \beta. \end{cases}$$

D.2 DETAILS FOR FIGURE 5 (B)

Augmentation Transformation Probability. Illustrated in Figure 5 (b), when semantic OOD and covariate OOD share the same domain, the augmentation matrix can be slightly different from the previous case:

$$\mathcal{T} = \begin{bmatrix} \rho & \beta & \alpha & \gamma & \gamma \\ \beta & \rho & \gamma & \alpha & \gamma \\ \alpha & \gamma & \rho & \beta & \beta \\ \gamma & \alpha & \beta & \rho & \beta \\ \gamma & \gamma & \beta & \beta & \rho \end{bmatrix}$$

Each row or column represents augmentation connectivity of a specific sample, ordered by: angel sketch, tiger sketch, angel painting, tiger painting, and panda.

Details for $A_1^{(u)}$ and $A_1^{(l)}$. After the assumption $\eta_u = 5, \eta_l = 1$, we can have $\eta_u A_1^{(u)} = \mathcal{T}\mathcal{T}^\top$:

$$\eta_u A_1^{(u)} = \begin{bmatrix} \rho^2+\beta^2+\alpha^2+2\gamma^2 & 2\rho\beta+\gamma^2+2\gamma\alpha & 2\rho\alpha+3\gamma\beta & 2\alpha\beta+\gamma\beta+2\gamma\rho & \alpha\beta+2\gamma(\beta+\rho) \\ 2\rho\beta+\gamma^2+2\gamma\alpha & \rho^2+\beta^2+\alpha^2+2\gamma^2 & 2\alpha\beta+\gamma\beta+2\gamma\rho & 2\rho\alpha+3\gamma\beta & \alpha\beta+2\gamma(\beta+\rho) \\ 2\rho\alpha+3\gamma\beta & 2\alpha\beta+\gamma\beta+2\gamma\rho & \rho^2+2\beta^2+\alpha^2+\gamma^2 & 2\rho\beta+\beta^2+2\gamma\alpha & 2\rho\beta+\beta^2+\gamma^2+\gamma\alpha \\ 2\alpha\beta+\gamma\beta+2\gamma\rho & 2\alpha\rho+3\gamma\beta & 2\rho\beta+\beta^2+2\gamma\alpha & \rho^2+2\beta^2+\alpha^2+\gamma^2 & 2\rho\beta+\beta^2+\gamma^2+\gamma\alpha \\ \alpha\beta+2\gamma(\beta+\rho) & \alpha\beta+2\gamma(\beta+\rho) & 2\rho\beta+\beta^2+\gamma^2+\gamma\alpha & 2\rho\beta+\beta^2+\gamma^2+\gamma\alpha & \rho^2+2\beta^2+2\gamma^2 \end{bmatrix}$$

And the supervised adjacency matrix $A_1^{(l)} = \mathcal{T}_{:,1}\mathcal{T}_{:,1}^\top + \mathcal{T}_{:,2}\mathcal{T}_{:,2}^\top$ can be given by:

$$\eta_l A_1^{(l)} = \begin{bmatrix} \rho^2+\beta^2 & 2\rho\beta & \rho\alpha+\gamma\beta & \alpha\beta+\gamma\rho & \gamma(\beta+\rho) \\ 2\rho\beta & \rho^2+\beta^2 & \alpha\beta+\gamma\rho & \rho\alpha+\gamma\beta & \gamma(\beta+\rho) \\ \rho\alpha+\gamma\beta & \alpha\beta+\gamma\rho & \alpha^2+\gamma^2 & 2\gamma\alpha & \gamma(\gamma+\alpha) \\ \alpha\beta+\gamma\rho & \rho\alpha+\gamma\beta & 2\gamma\alpha & \alpha^2+\gamma^2 & \gamma(\gamma+\alpha) \\ \gamma(\beta+\rho) & \gamma(\beta+\rho) & \gamma(\gamma+\alpha) & \gamma(\gamma+\alpha) & 2\gamma^2 \end{bmatrix}$$

Details for $\widehat{V}_1$. Following the same assumption, the adjacency matrix can be approximately given by:

$$A_1 \approx \widehat{A_1} = \frac{1}{\widehat{C_1}} \begin{bmatrix} 2 & 4\beta' & 3\alpha' & 0 & 0 \\ 4\beta' & 2 & 0 & 3\alpha' & 0 \\ 3\alpha' & 0 & 1 & 2\beta' & 2\beta' \\ 0 & 3\alpha' & 2\beta' & 1 & 2\beta' \\ 0 & 0 & 2\beta' & 2\beta' & 1 \end{bmatrix}$$

$$\widehat{D_1} = \frac{1}{\widehat{C_1}} \cdot \text{diag}[2+4\beta'+3\alpha', 2+4\beta'+3\alpha', 1+4\beta'+3\alpha', 1+4\beta'+3\alpha', 1+4\beta']$$

$$\widehat{D_1^{-\frac{1}{2}}} = \sqrt{\widehat{C_1}} \cdot \text{diag}[\frac{1}{\sqrt{2}}(1-\beta'-\frac{3}{4}\alpha'), \frac{1}{\sqrt{2}}(1-\beta'-\frac{3}{4}\alpha'), 1-2\beta'-\frac{3}{2}\alpha', 1-2\beta'-\frac{3}{2}\alpha', 1-2\beta']$$

$$D_1^{-\frac{1}{2}} A_1 D_1^{-\frac{1}{2}} \approx \widehat{D_1^{-\frac{1}{2}}}\widehat{A_1}\widehat{D_1^{-\frac{1}{2}}} = \begin{bmatrix} 1-2\beta'-\frac{3}{2}\alpha' & 2\beta' & \frac{3}{\sqrt{2}}\alpha' & 0 & 0 \\ 2\beta' & 1-2\beta'-\frac{3}{2}\alpha' & 0 & \frac{3}{\sqrt{2}}\alpha' & 0 \\ \frac{3}{\sqrt{2}}\alpha' & 0 & 1-4\beta'-3\alpha' & 2\beta' & 2\beta' \\ 0 & \frac{3}{\sqrt{2}}\alpha' & 2\beta' & 1-4\beta'-3\alpha' & 2\beta' \\ 0 & 0 & 2\beta' & 2\beta' & 1-4\beta' \end{bmatrix}$$

where $\widehat{C}_1$ is the normalization term and $\widehat{C}_1 = 7 + 20\beta' + 12\alpha'$. After eigendecomposition, we can derive ordered eigenvalues and their corresponding eigenvectors:

$$\widehat{v}_1 = \tfrac{1}{\sqrt{7}}[\sqrt{2}, \sqrt{2}, 1, 1, 1]^\top \qquad \widehat{\lambda}_1 = 1$$

$$\widehat{v}_2 = \tfrac{1}{\sqrt{2a(\widehat{\lambda}_2)^2+2b(\widehat{\lambda}_2)^2+1}}[a(\widehat{\lambda}_2), a(\widehat{\lambda}_2), b(\widehat{\lambda}_2), b(\widehat{\lambda}_2), 1]^\top \qquad \widehat{\lambda}_2 = 1-3b+\tfrac{\sqrt{3}\sqrt{(27a^2-40ab+48b^2)}-9a}{4}$$

$$\widehat{v}_3 = \tfrac{1}{\sqrt{2c(\widehat{\lambda}_3)^2+2}}[c(\widehat{\lambda}_3), -c(\widehat{\lambda}_3), -1, 1, 0]^\top \qquad \widehat{\lambda}_3 = 1-5b+\tfrac{\sqrt{81a^2+24ab+16b^2}-9a}{4}$$

$$\widehat{v}_4 = \tfrac{1}{\sqrt{2a(\widehat{\lambda}_4)^2+2b(\widehat{\lambda}_4)^2+1}}[a(\widehat{\lambda}_4), a(\widehat{\lambda}_4), b(\widehat{\lambda}_4), b(\widehat{\lambda}_4), 1]^\top \qquad \widehat{\lambda}_4 = 1-3b-\tfrac{\sqrt{3}\sqrt{(27a^2-40ab+48b^2)}+9a}{4}$$

$$\widehat{v}_5 = \tfrac{1}{\sqrt{2c(\widehat{\lambda}_5)^2+2}}[c(\widehat{\lambda}_5), -c(\widehat{\lambda}_5), -1, 1, 0]^\top, \qquad \widehat{\lambda}_5 = 1-5b-\tfrac{\sqrt{81a^2+24ab+16b^2}+9a}{4}$$

where $\widehat{\lambda}_1 > \widehat{\lambda}_2 > \widehat{\lambda}_3 > \widehat{\lambda}_4 > \widehat{\lambda}_5$ and $a(\lambda) = \frac{\sqrt{2}(1-6\beta'-\lambda)}{8\beta'}, b(\lambda) = \frac{4\beta'-1+\lambda}{4\beta'}, c(\lambda) = \frac{\sqrt{2}(1-3\alpha'-6\beta'-\lambda)}{3\alpha'}$. We can get closed-form eigenvectors:

$$\widehat{V}_1 = \begin{bmatrix} \sqrt{2} & \sqrt{2} & 1 & 1 & 1 \\ a(\widehat{\lambda}_2) & a(\widehat{\lambda}_2) & b(\widehat{\lambda}_2) & b(\widehat{\lambda}_2) & 1 \\ c(\widehat{\lambda}_3) & -c(\widehat{\lambda}_3) & -1 & 1 & 0 \end{bmatrix}^\top \cdot \text{diag}[\frac{1}{\sqrt{7}}, \frac{1}{\sqrt{2a(\widehat{\lambda}_2)^2 + 2b(\widehat{\lambda}_2)^2 + 1}}, \frac{1}{\sqrt{2c(\widehat{\lambda}_3)^2 + 2}}]$$

Details for linear probing and separability evaluation. Following the same derivation, we can derive closed-form embedding for ID samples $\widehat{Z}_{\text{in}} = \widehat{D_{\text{in}}^{-\frac{1}{2}}} \widehat{V}_{\text{in}} \sqrt{\widehat{\Sigma}_{\text{in}}}$ and the linear layer weights $\widehat{M} = (\widehat{Z}_{\text{in}}^\top \widehat{Z}_{\text{in}})^\dagger \widehat{Z}_{\text{in}}^T y_{\text{in}}$. Eventually, we can derive the approximately predicted probability $\hat{y}_{\text{out}}^{\text{covariate}}$:

$$\hat{y}_{\text{out}}^{\text{covariate}} = \begin{bmatrix} a_1 + b_1 & a_1 - b_1 \\ a_1 - b_1 & a_1 + b_1 \end{bmatrix}$$

where $a_1, b_1 \in \mathbb{R}$ and $b_1 > 0$. This indicates that linear probing error $\mathcal{E}(f_1) = 0$ as long as α and β are positive.

Having obtained closed-form representation Z_{in} and $Z_{\text{out}}^{\text{semantic}}$, we can compute separability $S(f_1)$ and then prove:

$$\widehat{Z}_{\text{in}} = \frac{(1 - \beta' - \frac{3}{4}\alpha')\sqrt{\widehat{C_1}}}{\sqrt{2}} \begin{bmatrix} \frac{\sqrt{2}}{\sqrt{7}} & \frac{a(\widehat{\lambda}_2)\sqrt{\widehat{\lambda}_2}}{\sqrt{2a(\widehat{\lambda}_2)^2+2b(\widehat{\lambda}_2)^2+1}} & -\frac{c(\widehat{\lambda}_3)\sqrt{\widehat{\lambda}_3}}{\sqrt{2c(\widehat{\lambda}_3)^2+2}} \\ \frac{\sqrt{2}}{\sqrt{7}} & \frac{a(\widehat{\lambda}_2)\sqrt{\widehat{\lambda}_2}}{\sqrt{2a(\widehat{\lambda}_2)^2+2b(\widehat{\lambda}_2)^2+1}} & \frac{c(\widehat{\lambda}_3)\sqrt{\widehat{\lambda}_3}}{\sqrt{2c(\widehat{\lambda}_3)^2+2}} \end{bmatrix}$$

$$\widehat{Z}_{\text{out}}^{\text{semantic}} = (1 - 2\beta')\sqrt{\widehat{C_1}}[\frac{1}{\sqrt{7}}, \frac{\sqrt{\widehat{\lambda}_2}}{\sqrt{2a(\widehat{\lambda}_2)^2 + 2b(\widehat{\lambda}_2)^2 + 1}}, 0]$$

$$\mathcal{S}(f) - \mathcal{S}(f_1) \begin{cases} > 0 & \text{, if } \alpha', \beta' \in \text{black area in Figure 6 (b);} \\ < 0 & \text{, if } \alpha', \beta' \in \text{white area in Figure 6 (b).} \end{cases}$$

D.3 Calculation Details for Self-Supervised Case

Our analysis for the self-supervised case is based on Figure 5 (a), the adjacency matrix is exactly the same as Eq. 10. After approximation, we can derive:

$$A^{(u)} \approx \widehat{A}^{(u)} = \frac{1}{\widehat{C}^{(u)}} \begin{bmatrix} 1 & 2\beta' & 2\alpha' & 0 & 0 \\ 2\beta' & 1 & 0 & 2\alpha' & 0 \\ 2\alpha' & 0 & 1 & 2\beta' & 0 \\ 0 & 2\alpha' & 2\beta' & 1 & 0 \\ 0 & 0 & 0 & 0 & 1 \end{bmatrix}$$

$$\widehat{D^{(u)}}^{-\frac{1}{2}} = \sqrt{5 + 8\beta' + 8\alpha'} \cdot \text{diag}[1 - \beta' - \alpha', 1 - \beta' - \alpha', 1 - \beta' - \alpha', 1 - \beta' - \alpha', 1]$$

$$\widehat{D^{(u)}}^{-\frac{1}{2}} \widehat{A^{(u)}} \widehat{D^{(u)}}^{-\frac{1}{2}} = \begin{bmatrix} 1 - 2\beta' - 2\alpha' & 2\beta' & 2\alpha' & 0 & 0 \\ 2\beta' & 1 - 2\beta' - 2\alpha' & 0 & 2\alpha' & 0 \\ 2\alpha' & 0 & 1 - 2\beta' - 2\alpha' & 2\beta' & 0 \\ 0 & 2\alpha' & 2\beta' & 1 - 2\beta' - 2\alpha' & 0 \\ 0 & 0 & 0 & 0 & 1 \end{bmatrix}$$

$$\begin{aligned} \widehat{v}_1 &= \tfrac{1}{2}[1, 1, 1, 1, 0]^\top & \widehat{\lambda}_1 &= 1 \\ \widehat{v}_2 &= [0, 0, 0, 0, 1]^\top & \widehat{\lambda}_2 &= 1 \\ \widehat{v}_3 &= \tfrac{1}{2}[-1, 1, -1, 1, 0]^\top & \widehat{\lambda}_3 &= 1 - 4\beta' \\ \widehat{v}_4 &= \tfrac{1}{2}[-1, -1, 1, 1, 0]^\top & \widehat{\lambda}_4 &= 1 - 4\alpha' \\ \widehat{v}_5 &= \tfrac{1}{2}[1, -1, -1, 1, 0]^\top & \widehat{\lambda}_5 &= 1 - 4\alpha' - 4\beta' \end{aligned}$$

Following the same procedure presented above, we can prove Theorem C.1 and C.2.

E MORE EXPERIMENTS

E.1 DATASET STATISTICS

We provide a detailed description of the datasets used in this work below:

CIFAR-10 (Krizhevsky et al., 2009) contains $60,000$ color images with 10 classes. The training set has $50,000$ images and the test set has $10,000$ images.

ImageNet-100 consists of a subset of 100 categories from ImageNet-1K (Deng et al., 2009). This dataset contains the following classes: n01498041, n01514859, n01582220, n01608432, n01616318, n01687978, n01776313, n01806567, n01833805, n01882714, n01910747, n01944390, n01985128, n02007558, n02071294, n02085620, n02114855, n02123045, n02128385, n02129165, n02129604, n02165456, n02190166, n02219486, n02226429, n02279972, n02317335, n02326432, n02342885, n02363005, n02391049, n02395406, n02403003, n02422699, n02442845, n02444819, n02480855, n02510455, n02640242, n02672831, n02687172, n02701002, n02730930, n02769748, n02782093, n02787622, n02793495, n02799071, n02802426, n02814860, n02840245, n02906734, n02948072, n02980441, n02999410, n03014705, n03028079, n03032252, n03125729, n03160309, n03179701, n03220513, n03249569, n03291819, n03384352, n03388043, n03450230, n03481172, n03594734, n03594945, n03627232, n03642806, n03649909, n03661043, n03676483, n03724870, n03733281, n03759954, n03761084, n03773504, n03804744, n03916031, n03938244, n04004767, n04026417, n04090263, n04133789, n04153751, n04296562, n04330267, n04371774, n04404412, n04465501, n04485082, n04507155, n04536866, n04579432, n04606251, n07714990, n07745940.

CIFAR-10-C is generated based on Hendrycks & Dietterich (2018), applying different corruptions on CIFAR-10 including gaussian noise, defocus blur, glass blur, impulse noise, shot noise, snow, and zoom blur.

ImageNet-100-C is generated with Gaussian noise added to ImageNet-100 dataset (Deng et al., 2009).

SVHN (Netzer et al., 2011) is a real-world image dataset obtained from house numbers in Google Street View images. This dataset $73,257$ samples for training, and $26,032$ samples for testing with 10 classes.

Places365 (Zhou et al., 2017) contains scene photographs and diverse types of environments encountered in the world. The scene semantic categories consist of three macro-classes: Indoor, Nature, and Urban.

LSUN-C (Yu et al., 2015) and **LSUN-R** (Yu et al., 2015) are large-scale image datasets that are annotated using deep learning with humans in the loop. LSUN-C is a cropped version of LSUN and LSUN-R is a resized version of the LSUN dataset.

Textures (Cimpoi et al., 2014) refers to the Describable Textures Dataset, which contains a large dataset of visual attributes including patterns and textures. The subset we used has no overlap categories with the CIFAR dataset (Krizhevsky et al., 2009).

iNaturalist (Horn et al., 2018) is a challenging real-world dataset with iNaturalist species, captured in a wide variety of situations. It has 13 super-categories and 5,089 sub-categories. We use the subset from Huang & Li (2021) that contains 110 plant classes that no category overlaps with IMAGENET-1K (Deng et al., 2009).

Office-Home (Venkateswara et al., 2017) is a challenging dataset, which consists of 15500 images from 65 categories. It is made up of 4 domains: Artistic (Ar), Clip-Art (Cl), Product (Pr), and Real-World (Rw).

Details of data split for OOD datasets. For datasets with standard train-test split (e.g., SVHN), we use the original test split for evaluation. For other OOD datasets (e.g., LSUN-C), we use 70% of the data for creating the wild mixture training data as well as the mixture validation dataset. We use the remaining examples for test-time evaluation. For splitting training/validation, we use 30% for validation and the remaining for training. During validation, we could only access unlabeled wild data and labeled clean ID data, which means hyper-parameters are chosen based on the performance of ID Acc. on the ID validation set (more in Section F).

Model	Places365 $\mathbb{P}_{\text{out}}^{\text{semantic}}$, CIFAR-10-C $\mathbb{P}_{\text{out}}^{\text{covariate}}$				LSUN-R $\mathbb{P}_{\text{out}}^{\text{semantic}}$, CIFAR-10-C $\mathbb{P}_{\text{out}}^{\text{covariate}}$			
	OOD Acc.↑	ID Acc.↑	FPR↓	AUROC↑	OOD Acc.↑	ID Acc.↑	FPR↓	AUROC↑
OOD detection								
MSP	75.05	94.84	57.40	84.49	75.05	94.84	52.15	91.37
ODIN	75.05	94.84	57.40	84.49	75.05	94.84	26.62	94.57
Energy	75.05	94.84	40.14	89.89	75.05	94.84	27.58	94.24
Mahalanobis	75.05	94.84	68.57	84.61	75.05	94.84	42.62	93.23
ViM	75.05	94.84	**21.95**	**95.48**	75.05	94.84	36.80	93.37
KNN	75.05	94.84	42.67	91.07	75.05	94.84	29.75	94.60
ASH	75.05	94.84	44.07	88.84	75.05	94.84	22.07	95.61
OOD generalization								
IRM	77.92	90.85	53.79	88.15	77.92	90.85	34.50	94.54
GroupDRO	77.27	**94.97**	32.81	91.85	77.27	94.97	14.60	97.04
Mixup	79.17	93.30	58.24	75.70	79.17	93.30	32.73	88.86
VREx	76.90	91.35	56.13	87.45	76.90	91.35	44.20	92.55
EQRM	75.71	92.93	51.00	88.61	75.71	92.93	31.23	94.94
SharpDRO	79.03	94.91	34.64	91.96	79.03	94.91	13.27	97.44
Learning w. $\mathbb{P}_{wild}$								
OE	35.98	94.75	27.02	94.57	46.89	94.07	0.70	99.78
Energy (w/ outlier)	19.86	90.55	23.89	93.60	32.91	93.01	0.27	99.94
Woods	54.58	94.88	30.48	93.28	78.75	**95.01**	0.60	99.87
Scone	85.21	94.59	37.56	90.90	**80.31**	94.97	0.87	99.79
SLW (Ours)	**87.04**$_{\pm 0.3}$	93.40$_{\pm 0.3}$	40.97$_{\pm 1.1}$	91.82$_{\pm 0.0}$	79.38$_{\pm 0.8}$	92.44$_{\pm 0.1}$	**0.06**$_{\pm 0.0}$	**99.99**$_{\pm 0.0}$

Table 2: Additional results: comparison with competitive OOD generalization and OOD detection methods on CIFAR-10. To facilitate a fair comparison, we include results from Bai et al. (2023) and set $\pi_c = 0.5, \pi_s = 0.1$ by default for the mixture distribution $\mathbb{P}_{\text{wild}} := (1 - \pi_s - \pi_c)\mathbb{P}_{\text{in}} + \pi_s \mathbb{P}_{\text{out}}^{\text{semantic}} + \pi_c \mathbb{P}_{\text{out}}^{\text{covariate}}$. **Bold**=best. (*Since all the OOD detection methods use the same model trained with the CE loss on $\mathbb{P}_{\text{in}}$, they display the same ID and OOD accuracy on CIFAR-10-C.)

E.2 Results on ImageNet-100

In this section, we present results on the large-scale dataset ImageNet-100 to further demonstrate our empirical competitive performance. We employ ImageNet-100 as $\mathbb{P}_{\text{in}}$, ImageNet-100-C as $\mathbb{P}_{\text{out}}^{\text{covariate}}$, and iNaturalist (Horn et al., 2018) as $\mathbb{P}_{\text{out}}^{\text{semantic}}$. Similar to our CIFAR experiment, we divide the ImageNet-100 training set into 50% labeled as ID and 50% unlabeled. Then we mix unlabeled ImageNet-100, ImageNet-100-C, and iNaturalist to generate the wild dataset. We include results from Bai et al. (2023) and set $\pi_c = 0.5, \pi_s = 0.1$ for consistency. We pre-train the backbone ResNet-34 (He et al., 2016) with SLW and then use ID data to fine-tune the model. We set the pre-training epoch as 100, batch size as 512, and learning rate as 0.01. For fine-tuning, we set the learning rate to 0.01, batch size to 128, and train for 10 epochs. Empirical results in Table 3 indicate that our method effectively balances OOD generalization and detection while achieving strong performance in both aspects. While Wood (Katz-Samuels et al., 2022) displays strong OOD detection performance, the OOD generation performance (44.46%) is significantly worse than ours (72.58%). More detailed implementation can be found in Appendix F.

Method	OOD Acc.↑	ID Acc.↑	FPR↓	AUROC↑
Woods	44.46	86.49	**10.50**	**98.22**
Scone	65.34	**87.64**	27.13	95.66
SLW (Ours)	**72.58**	86.68	21.00	96.52

Table 3: Results on ImageNet-100. We employ ImageNet-100 as $\mathbb{P}_{\text{in}}$, ImageNet-100-C with Gaussian noise as $\mathbb{P}_{\text{out}}^{\text{covariate}}$, and iNaturalist as $\mathbb{P}_{\text{out}}^{\text{semantic}}$. **Bold**=Best.

E.3 Results on Office-Home

In this section, we present empirical results on the Office-Home (Venkateswara et al., 2017), a dataset comprising 65 object classes distributed across 4 different domains: Artistic (Ar), Clipart (Cl), Product (Pr), and Real-World (Rw). Following Saito et al. (2018), we separate 65 object classes into the first 25 classes in alphabetic order as ID classes and the remainder of classes as semantic OOD classes. Subsequently, we construct the ID data from one domain (e.g., Ar) across 25 classes,

and the covariate OOD from another domain (e.g., Cl) to carry out the OOD generalization task (e.g., Ar $\rightarrow$ Cl). The semantic OOD data are from the remainder of classes, in the same domain as covariate OOD data. We consider the following wild data, where $\mathbb{P}_{\text{wild}} = \pi_c \mathbb{P}_{\text{out}}^{\text{covariate}} + \pi_s \mathbb{P}_{\text{out}}^{\text{semantic}}$ and $\pi_c + \pi_s = 1$. This setting is also known as open-set domain adaptation (Panareda Busto & Gall, 2017), which can be viewed as a special case of ours.

For a fair empirical comparison, we include results from Li et al. (2023), containing comprehensive baselines like STA (Liu et al., 2019), OSBP (Saito et al., 2018), DAOD (Fang et al., 2021), OSLPP (Wang et al., 2021b), ROS (Bucci et al., 2020), and Anna (Li et al., 2023). Following previous literature, we use OOD Acc. to denote the average class accuracy over known classes only in this section. We employ ResNet-50 (He et al., 2016) as the default backbone. As shown in Table 4, our approach strikes a balance between OOD generalization and detection, even outperforming the state-of-the-art method Anna in terms of FPR by 11.3% on average. This demonstrates the effectiveness of our method in handling the complex OOD scenarios present in the Office-Home dataset. More detailed implementation can be found in Appendix F.

Method	Ar → Cl		Ar → Pr		Ar → Rw		Cl → Ar		Cl → Pr		Cl → Rw		Pr → Ar	
	OOD Acc.↑	FPR↓	OOD Acc.↑	FPR↓	OOD Acc.↑	FPR↓	OOD Acc.↑	FPR↓	OOD Acc.↑	FPR↓	OOD Acc.↑	FPR↓	OOD Acc.↑	FPR↓
STA$_{\text{sum}}$	50.8	36.6	68.7	40.3	**81.1**	49.5	53.0	36.1	61.4	36.5	69.8	36.8	55.4	26.3
STA$_{\text{max}}$	46.0	27.7	68.0	51.6	78.6	39.6	51.4	35.0	61.8	40.9	67.0	33.3	54.2	27.6
OSBP	50.2	38.9	71.8	40.2	79.3	32.5	**59.4**	29.7	67.0	37.3	72.0	30.8	59.1	31.9
DAOD	**72.6**	48.2	55.3	42.1	78.2	37.4	59.1	38.3	**70.8**	47.4	**77.8**	43.0	**71.3**	49.5
OSLPP	55.9	32.9	**72.5**	26.9	80.1	30.6	49.6	21.0	61.6	26.7	67.2	26.1	54.6	23.8
ROS	50.6	25.9	68.4	29.7	75.8	22.8	53.6	34.5	59.8	28.4	65.3	27.8	57.3	35.7
Anna	61.4	21.3	68.3	20.1	74.1	20.3	58.0	26.9	64.2	26.4	66.9	19.8	63.0	29.7
SLW (Ours)	54.2	**14.1**	68.7	**12.7**	78.6	**15.8**	51.1	**14.8**	61.0	**8.8**	68.0	**10.5**	58.3	**9.2**

Method	Pr → Cl		Pr → Rw		Rw → Ar		Rw → Cl		Rw → Pr		Average	
	OOD Acc.↑	FPR↓	OOD Acc.↑	FPR↓	OOD Acc.↑	FPR↓	OOD Acc.↑	FPR↓	OOD Acc.↑	FPR↓	OOD Acc.↑	FPR↓
STA$_{\text{sum}}$	44.7	28.5	78.1	36.7	**67.9**	37.7	51.4	42.1	77.9	42.0	63.4	37.4
STA$_{\text{max}}$	44.2	32.9	76.2	35.7	67.5	33.3	49.9	38.9	77.1	44.6	61.8	36.7
OSBP	44.5	33.7	76.2	28.3	66.1	32.7	48.0	37.0	76.3	31.4	64.1	33.7
DAOD	**58.4**	57.2	**81.8**	49.4	66.7	56.7	**60.0**	63.4	**84.1**	65.3	**69.6**	49.8
OSLPP	53.1	32.9	77.0	28.8	60.8	25.0	54.4	35.7	78.4	29.2	63.8	28.3
ROS	46.5	28.8	70.8	21.6	67.0	29.2	51.5	27.0	72.0	20.0	61.6	27.6
Anna	54.6	25.2	74.3	21.1	66.1	22.7	59.7	26.9	76.4	19.0	65.6	23.3
SLW (Ours)	48.1	**13.4**	76.9	**8.00**	64.8	**9.5**	56.1	**11.8**	80.9	**14.5**	63.9	**12.0**

Table 4: Results on Office-Home. **Bold**=Best.

E.4 Ablation Study

Impacts of ID labels. As shown in Table 5, we contrast performance by pre-training with and without ID labels. The wild data follows the same setting as our main paper, which is a composition of CIFAR-10, CIFAR-10-C, and one of the five semantic OOD datasets. By comparing OOD accuracy and FPR, we find that the use of ID labels during pre-training significantly improves both OOD generalization and OOD detection, which aligns with our theoretical analysis.

$\mathbb{P}_{\text{out}}^{\text{semantic}}$	ID labels	OOD Acc.↑	ID Acc.↑	FPR↓	AUROC↑
SVHN	✗	62.02	80.26	20.64	96.44
	✓	**86.62**	**93.10**	**0.13**	**99.98**
LSUN-C	✗	67.59	83.35	57.70	88.83
	✓	**85.88**	**92.61**	**1.76**	**99.75**
TEXTURES	✗	64.47	76.78	75.66	78.32
	✓	**81.40**	**92.50**	**12.05**	**98.25**
PLACES365	✗	70.76	81.48	66.40	83.15
	✓	**87.04**	**93.40**	**40.97**	**91.82**
LSUN-R	✗	63.09	74.25	40.50	90.24
	✓	**79.68**	**92.44**	**0.06**	**99.99**

Table 5: Impact of ID labels during pre-training. We employ CIFAR-10 as $\mathbb{P}_{\text{in}}$ and CIFAR-10-C with Gaussian noise as $\mathbb{P}_{\text{out}}^{\text{covariate}}$. **Bold**=Best.

Impact of semantic OOD data. Table 6 empirically verifies the theoretical analysis in Section B. We follow Cao et al. (2022) and separate classes in CIFAR-10 into 50% known and 50% unknown classes. To demonstrate the impacts of semantic OOD data on generalization, we simulate scenarios when semantic OOD shares the same or different domain as covariate OOD. Empirical results in Table 6 indicate that when semantic OOD shares the same domain as covariate OOD, it could significantly improve the performance of OOD generalization.

Corruption Type of $\mathbb{P}_{\text{out}}^{\text{covariate}}$	$\mathbb{P}_{\text{out}}^{\text{semantic}}$	OOD Acc.↑
Gaussian noise	SVHN	85.48
Gaussian noise	LSUN-C	85.88
Gaussian noise	Places365	83.28
Gaussian noise	Textures	86.84
Gaussian noise	LSUN-R	80.08
Gaussian noise	Gaussian noise	**88.18**

Table 6: The impact of semantic OOD data on generalization. Classes in CIFAR-10 are divided into 50% known and 50% unknown classes. The experiment in the last line uses known classes in CIFAR-10-C with Gaussian noise as $\mathbb{P}_{\text{out}}^{\text{covariate}}$ and novel classes in CIFAR-10-C with Gaussian noise as $\mathbb{P}_{\text{out}}^{\text{semantic}}$. **Bold**=best.

F Implementation Details

Training settings. We conduct all the experiments in Pytorch, using NVIDIA GeForce RTX 2080Ti. We use SGD optimizer with weight decay 5e-4 and momentum 0.9 for all the experiments. In CIFAR-10 experiments, we pre-train Wide ResNet with SLW loss for 1000 epochs. The learning rate (lr) is 0.030, batch size (bs) is 512. Then we use ID-labeled data to fine-tune for 20 epochs with lr 0.005 and bs 512. In ImageNet-100 experiments, we train ImageNet pre-trained ResNet-34 with SLW loss for 100 epochs. The lr is 0.01, bs is 512. Then we fine-tune for 10 epochs with lr 0.01 and bs 128. In Office-Home experiments, we use ImageNet pre-trained ResNet-50 with lr 0.001 and bs 64. We use the same data augmentation strategies as SimSiam (Chen & He, 2021). We set K in KNN as 50 in CIFAR-10 experiments and 100 in ImageNet-100 experiments, which is consistent with Sun et al. (2022). And η_u is selected within $\{1.00, 2.00\}$ and η_l is within $\{0.02, 0.10, 0.50, 1.00\}$. In Office-Home experiments, we set K as 5, η_u as 3, and η_l within $\{0.01, 0.05\}$. η_u, η_l are summarized in Table 7.

ID/Covariate OOD	Semantics OOD	η_l	η_u
CIFAR-10/CIFAR-10-C	SVHN	0.50	2.00
CIFAR-10/CIFAR-10-C	LSUN-C	0.50	2.00
CIFAR-10/CIFAR-10-C	Textures	0.50	1.00
CIFAR-10/CIFAR-10-C	Places365	0.50	2.00
CIFAR-10/CIFAR-10-C	LSUN-R	0.10	2.00
ImageNet-100/ImageNet-100-C	iNaturalist	0.10	2.00
Office-Home Ar/Cl, Pr, Rw	Cl, Pr, Rw	0.01	3.00
Office-Home Cl/Ar, Pr, Rw	Ar, Pr, Rw	0.01	3.00
Office-Home Pr/Ar, Cl, Rw	Ar, Cl, Rw	0.05	3.00
Office-Home Rw/Ar, Cl, Pr	Ar, Cl, Pr	0.05	3.00

Table 7: Selection of hyper-parameters η_l, η_u

Validation strategy. For validation, we could only access to unlabeled mixture of validation wild data and clean validation ID data, which is rigorously adhered to Bai et al. (2023). Hyper-parameters are chosen based on the performance of ID Acc. on the ID validation set. We present the sweeping results in Table 8.

η_l	η_u	ID Acc. (validation)↑	ID Acc.↑	OOD Acc.↑	FPR↓	AUROC↑
0.02	2.00	88.52	87.12	70.31	52.16	90.03
0.10	2.00	95.36	91.72	77.98	20.20	96.85
0.50	2.00	95.72	91.79	78.23	17.66	97.26
1.00	2.00	94.96	90.91	81.92	24.99	94.82
0.02	1.00	89.04	87.44	60.60	46.01	92.01
0.10	1.00	93.92	90.70	74.58	21.50	96.83
0.50	1.00	**96.76**	92.50	81.40	12.05	98.25
1.00	1.00	94.24	90.77	65.58	14.00	97.27

Table 8: Sensitivity analysis of hyper-parameters η_l, η_u. We employ CIFAR-10 as $\mathbb{P}_{\text{in}}$, CIFAR-10-C as $\mathbb{P}_{\text{out}}^{\text{covariate}}$, and Textures as $\mathbb{P}_{\text{out}}^{\text{semantic}}$. **Bold**=best.